Acta Cryst. (1980). A**36**, 1033–1041

Many-Beam Lattice Images Calculated at 100 kV and 1000 kV

BY M. TANAKA AND B. JOUFFREY

Laboratoire d'Optique Electronique du CNRS, Laboratoire Propre du CNRS associé à l'Université Paul Sabatier, 29 rue Jeanne Marvig, BP 4347, 31055 *Toulouse CEDEX, France*

(*Received* 2 *January* 1980; *accepted* 9 *July* 1980)

Abstract

Lattice images of high-temperature-phase vanadium sesquioxide (V_2O_3) were calculated within the Bloch-wave approach. At an accelerating voltage of 1000 kV the structure image can be produced while at 100 kV it cannot be obtained because of the small number of reflections available in the image formation, which demonstrates clearly an advantage of high voltages which are produced by improvement in the transfer condition of the objective lens. On the other hand, if an ideal phase-contrast lens is assumed in order to obtain the structure image at 100 kV, lattice-image calculations can be carried out with modified unit-cell size. The results show that the maximum allowable thickness to obtain the structure image varies more rapidly than in a linear manner with the required resolution. The maximum allowable thickness increases either with higher voltages (from about 20 Å at 100 kV to about 35 Å at 1000 kV) or with larger unit cells (*e.g.* a dilatation of 25% in unit-cell size increases the maximum thickness from about 20 to about 35 Å). However, the evolution of the image details as a function of crystal thickness is different for these two factors, due to the different dynamical interactions of electron waves.

1. Introduction

One of the great interests of high-resolution electron microscopy is that it enables us to obtain structural information localized at atomic scale in the specimen. However, because of the nature of the interaction between an electron beam and specimens and that of the electron-optical system, the mechanism giving the contrast in a high-resolution image is generally so complicated that it is not always possible to obtain from it reliable and useful information on the specimen structure. For this purpose, the image must bear one-to-one correspondence with, or at least must reflect directly, the specimen structure projected in the observation direction, *i.e.* it must be the 'structure image'. The conditions which must be fulfilled to obtain the structure image consist of the instrumental factors and the nature of the specimen. In the case of a weak phase object, for example, the image formed under the optimum defocus condition (Scherzer, 1949) will reflect directly the projected potential of the specimen, at least in so far as the spatial frequencies contained in the main transfer interval of the phase-contrast transfer function (Hanszen, 1971) are concerned. Firstly, structure images were obtained from thin crystalline specimens and were given a semiquantitative explanation by the weak-phase-object approximation (see Cowley & Iijima, 1972). It is also known that images taken under the above-mentioned condition from some complex oxide crystals of large unit cell show the structure image in a relatively thick region, where the crystal cannot be considered as being a weak phase object, as well as in the very thin region (Fejes, Iijima & Cowley, 1973). This phenomenon of recurrence of the same image as a function of the crystal thickness has also been reported for crystalline silicon (Rez & Krivanek, 1978; Spence, O'Keefe & Iijima, 1978) and vanadium sesquioxide (Tanaka, Rocher, Ayroles & Jouffrey, 1978). In order to foresee at what thicknesses the structure image recurs, it is necessary to know *a priori* the precise structure of the crystal and this condition will limit the applicability of the technique, whereas in the case of a weak phase object no such knowledge will, in principle, be needed. However, the specimen should be very thin so that it may be considered as a weak phase object. The problem is, thus, to evaluate the maximum thickness up to which a specimen can be treated in the weak-phase-object approximation. Naturally, the answer will be variable depending on the electrostatic potential of the specimen which encounters the electron beam, *i.e.* the thickness will depend both on the atoms constituting the specimen and on their arrangement. For instance, for graphitic carbon, Jefferson, Millward & Thomas (1976) estimate that the limit of thickness is less than 50 Å, and for $Ti_2Nb_{10}O_{29}$, Fejes (1977) gives a limit of less than *ca* 6 Å. Moreover, it appears that the weak-phase-object approximation is valid for thicknesses at which the crystal should no longer be a weak phase object (Fejes, 1977).

In the present paper are described the lattice images

0567-7394/80/061033-09$01.00

of a vanadium sesquioxide (V_2O_3) crystal which were calculated with the N-beam dynamical theory. Vanadium sesquioxide was chosen because it has a relatively small unit cell and contains different kinds of atoms whose scattering factors are considerably different. This will indicate if it is possible to visualize the columns of vanadium atoms and those of oxygen atoms individually, rather than observing groups of atoms as has been done with crystals of large-unit-cell complex oxides. Our intention is to observe the behaviour of the maximum allowable thickness in order to obtain the structure image from a thin crystal in two cases: (*a*) when different accelerating voltages of electrons are used, *i.e.* 100 kV and 1000 kV; and (*b*) when the unit cell is modified in size, *i.e.* dilatation or contraction of the lattice.

2. Method of image calculation

Lattice images were calculated with the Bloch-wave formulation of electron diffraction. The image amplitude for a perfect crystal can, then, be expressed as follows, apart from a constant phase factor common to all reflections:

$$\psi_{z,\Delta f}(\mathbf{r}) = \sum_{g}^{n} \sum_{j}^{N} C_0^{(j)} C_g^{(j)} \exp 2\pi i[(\gamma^{(j)} + iq^{(j)})z + \mathbf{g}.\mathbf{r}] \times \exp[-i\chi_{g,\Delta f}].$$

It is supposed that the crystal is in the form of a parallel plate of thickness z and that the incident electron beam is perpendicular to the crystal surface. n is the number of beams which pass through the objective aperture and thus form the image. $C_g^{(j)}$, $\gamma^{(j)}$ and $q^{(j)}$ are respectively the gth component of the jth eigenvector, the jth eigenvalue and the corresponding absorption coefficient. In the calculation of structure factors, the analytical approximation to electron scattering factors given by Doyle & Turner (1968) was used. For the absorption effect, the thermal diffuse scattering was considered in the perturbation approximation (Hirsch, Howie, Nicholson, Pashley & Whelan, 1965). The Fourier coefficients (V_g^i) of the imaginary crystal potential were calculated by a method analogous to those given by Hall & Hirsch (1965) and Radi (1970), using the atom form factors for X-rays given by Hanson, Herman, Lea & Skillman (1964). The Debye temperature of the vanadium sesquioxide was taken to be 630 K (Andrianov & Drichko, 1976) in estimating the mean square displacement of atoms in the crystal. The temperature of the crystal under observation in the microscope was supposed to be 400 K in consideration of the beam heating. However, for the mean absorption potential (V_o^i) the value of 0·69 V was used, which was determined from the damping of equal-thickness fringes obtained experimentally in a two-beam case. $\chi_{g,\Delta f}$ designates the phase shift introduced in the scattered wave by the spherical aberration (constant C_s) and the defocus (Δf) of the objective lens and can be expressed in terms of the scattering angle α_g associated with the reflection g:

$$\chi_{g,\Delta f} = \frac{\pi}{2\lambda}(C_s\alpha_g^4 - 2\Delta f\alpha_g^2),$$

where a positive value of Δf corresponds to underfocusing. The Schrödinger equation adopted in solving the diffraction problem gives for the incident wave exp $2\pi i(\mathbf{k}_0.\mathbf{r} - \omega t)$. The lattice image, $I_{z,\Delta f}(\mathbf{r}) = |\psi_{z,\Delta f}(\mathbf{r})|^2$, was calculated in the [2$\bar{2}$01] zone-axis* orientation with axial illumination. The objective aperture is assumed to be circular and centred on the optic axis of the microscope.

The high-temperature phase of vanadium sesquioxide is metallic and belongs to space group $R\bar{3}c$. The unit cell determined by Dernier (1970) in the hexagonal system contains six molecules and has the parameters $a = 4{\cdot}9515$ and $c = 14{\cdot}003$ Å.† Fig. 1 shows the electron

* This is not the principal axis in the high-temperature phase but contains the maximum number of largest lattice spacings. This orientation becomes parallel to [100] in the low-temperature monoclinic phase to which the crystal belongs below 150 K.

† The parameters for the rhombohedral cell derived from those of the hexagonal one are $a_R = 5{\cdot}4728$ Å, $\alpha = 53{\cdot}79°$.

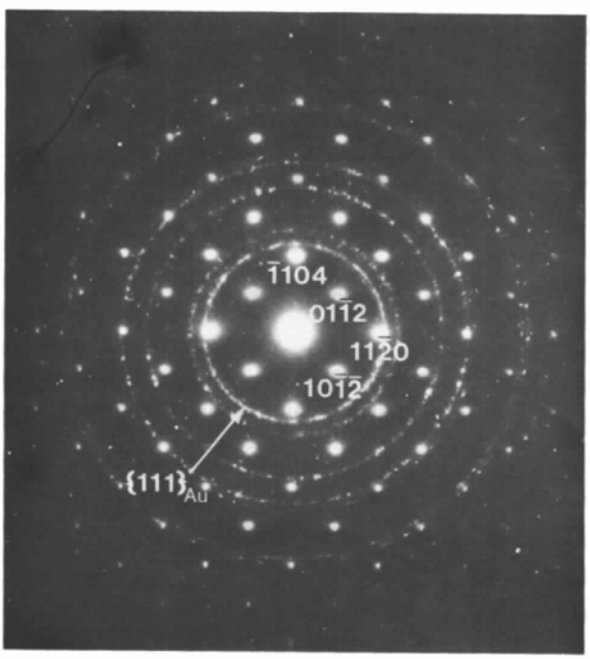

Fig. 1. Electron diffraction pattern obtained at 100 kV from a [2$\bar{2}$01]-oriented V_2O_3 crystal (space group $R\bar{3}c$) supported on a holey polycrystalline gold film, which produces the rings.

Table 1. *Some lowest reflections belonging to the* [2$\bar{2}$01] *zone axis of* V_2O_3 (*space group* $R\bar{3}c$) *and the corresponding lattice spacings*

Lattice spacings (Å)	Reflections
3·657	$10\bar{1}\bar{2}$ $01\bar{1}2$ $\bar{1}012$ $0\bar{1}1\bar{2}$
2·712	$1\bar{1}0\bar{4}$ $\bar{1}104$
2·476	$11\bar{2}0$ $\bar{1}\bar{1}20$
1·828	$20\bar{2}\bar{4}$ $02\bar{2}4$ $\bar{2}024$ $0\bar{2}2\bar{4}$
1·698	$1\bar{2}1\bar{6}$ $2\bar{1}\bar{1}6$ $\bar{1}2\bar{1}6$ $\bar{2}116$
1·579	$21\bar{3}\bar{2}$ $12\bar{3}2$ $\bar{2}132$ $\bar{1}2\bar{3}\bar{2}$
1·356	$22\bar{0}\bar{8}$ $\bar{2}208$
1·238	$22\bar{4}0$ $\bar{2}\bar{2}40$

diffraction pattern obtained from a [2$\bar{2}$01]-oriented crystal supported on a holey, polycrystalline gold film from which the diffraction rings arise. The indices of some low-order reflections which belong to this zone axis are listed in Table 1 in decreasing order of lattice spacing.

3. Results and discussion

3.1. *Determination of the number of reflections in the scattering matrix*

At an accelerating voltage of 100 kV, the distribution of reflections over the value of the parameter of the excitation error, $W = s\xi_g$, is shown by the histogram in Fig. 2(*a*). Fig. 3(*a*) shows equal-thickness fringes in the bright-field image, $I_{000}(z)$, calculated with three different numbers N (arrowed in the histogram) of reflections in the scattering matrix: (*a*) $N = 51$ (there are 51 reflections whose values of W are equal or inferior to 90), (*b*) $N = 65$ ($0 \leq W \leq 130$) and (*c*) $N = 90$ ($0 \leq W \leq 170$). The differences in intensity between the cases (*b*) and (*c*) are 15% at most for crystal thicknesses less than 200 Å. As will be seen in the following sections the thickness series of images calculated with 65 reflections (Fig. 10, third column from the left) and with 90 reflections (Fig. 4*c*) cannot be distinguished, indicating that 65 reflections can be considered practically sufficient at 100 kV for small-thickness regions.

The distribution of reflections at 1000 kV is shown in Fig. 2(*b*). It appears from the form of this histogram that $N \simeq 120$ is sufficient. The maximum value of W is then of the same order as that in the 65-reflection calculation at 100 kV. In order to avoid the diagonalization of very large scattering matrices, the profiles of the equal-thickness fringes were calculated in the case of $10\bar{1}\bar{2}$ systematic reflections at the symmetric incidence. Fig. 3(*b*) shows the intensity profile calculated with 11 reflections and the percentage deviation from the intensity calculated with 19 reflections which must be largely sufficient for the scattering matrix because the maximum value of W attains, then, 600. The deviation stays well below 1%, and it is certainly smaller than 0·1% for crystal thickness less than 100 Å. Therefore, 11 reflections are practically sufficient in the systematic case and so 121 reflections will be required in the [2$\bar{2}$01] zone-axis orientation containing the systematic row of reflections (see Fig. 1). In the lattice-image calculations for 1000 kV, 125 reflections were used for convenience.

3.2. *Effect of the accelerating voltage on the lattice-image contrast*

3.2.1. *Images at Scherzer defocus.* Fig. 4(*a*) shows a series of images calculated in the zone-axis orientation at different crystal thicknesses at 1000 kV with $C_s = 4{\cdot}2$ mm. The defocus value Δf is that of Scherzer, namely $1{\cdot}2(C_s\lambda)^{1/2} = 720$ Å. The transfer function has, for the imaginary part sin χ_g, the form shown in Fig. 5(*a*) (the real part is also included in the image calculations). The main transfer interval contains the

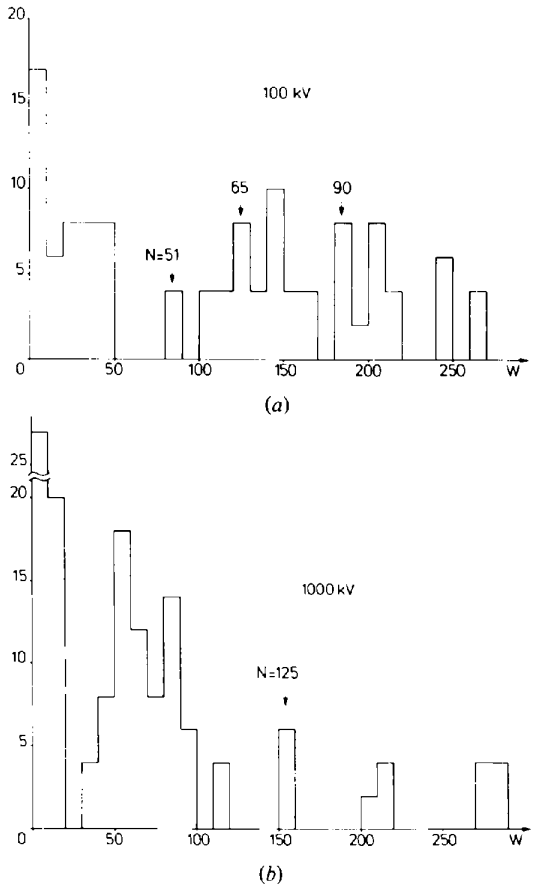

Fig. 2. Histogram showing the distribution of reflections of a [2$\bar{2}$01]-oriented V_2O_3 crystal over the parameter of excitation error (W). The ordinate gives the number of reflections. The values of N indicate the total number of reflections whose W are contained between 0 and the position of each arrow. (*a*) 100 kV. (*b*) 1000 kV.

smallest six spatial frequencies of the crystal in the orientation studied. The size of the objective aperture was chosen so that all these spatial frequencies ($n = 21$ reflections in total) could pass through and form the image. The projected structure of the crystal is shown in Fig. 4(*d*): dots and circles represent columns of vanadium atoms and those of oxygen atoms, respectively. When the crystal is thin enough, the image reflects directly the projected structure with normal contrast (Spence, O'Keefe & Kolar, 1977) as can be expected from the weak-phase-object approximation: a large dark dot corresponds to one column of vanadium atoms accompanied by two nearest-neighbour columns of oxygen atoms, and a small faint dot corresponds to a third column of oxygen atoms. As the crystal becomes thicker the contrast increases, but at a thickness of about 40 Å, the image begins to distort and it is no longer the structure image. Fig. 4(*b*) shows a series of images calculated with $N = 90$ at 100 kV and with $C_s = 0{\cdot}7$ mm. The defocus value is $\Delta f = 1180$ Å. The corresponding sin χ_g curve is shown in Fig. 5(*b*). The main transfer interval is then due to $\chi_g \simeq -5\pi/2$ and contains the smallest three spatial frequencies instead of only one (the smallest frequency) at ordinary Scherzer defocus giving $\chi_g \simeq -\pi/2$. The size of the objective aperture was fitted to the cut-off frequency, *i.e.* $1/2{\cdot}4$ Å^{-1}. The resolution in the calculated images is poor: the neighbouring columns of vanadium atoms separated by about 2 Å are not resolved, the column of oxygen atoms is not seen, and the white regions do not correspond to the tunnel sites in the projected structure. It may be noted that the result of this comparison between 100 and 1000 kV images is similar to that obtained by Fields & Cowley (1978) for a crystal having a unit cell derived from that of gold. Fig. 4(*c*) shows another series of images calculated at 100 kV and with $N = 90$. The transfer condition used is such

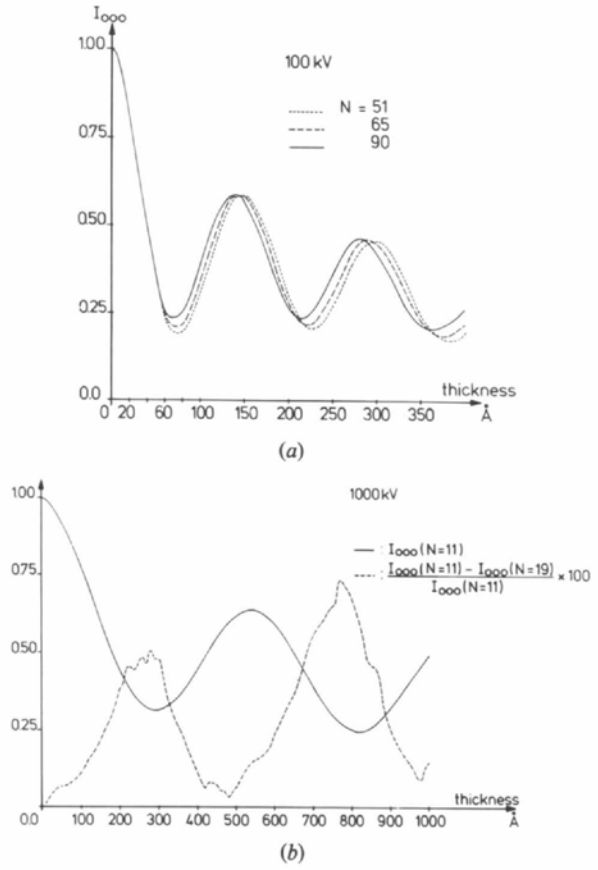

Fig. 3. Intensity profiles of the bright-field equal-thickness fringes calculated for (*a*) [2$\bar{2}$01] zone-axis orientation at 100 kV with the three different values of N indicated in Fig. 2(*a*), and (*b*) 10$\bar{1}\bar{2}$ systematic case at 1000 kV with symmetric incidence; solid line is the intensity calculated with $N = 11$; broken line is the percentage deviation from $N = 11$ calculation of the intensity calculated with $N = 19$.

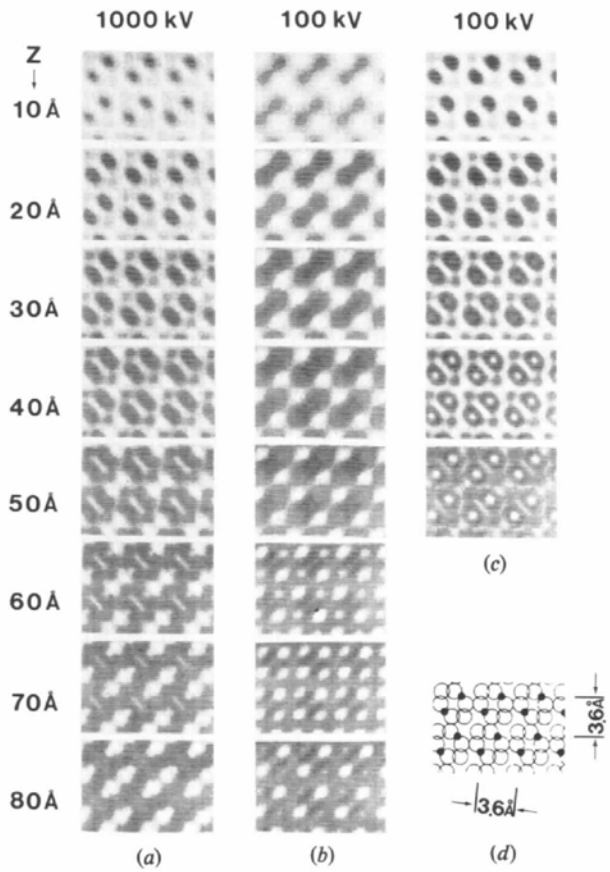

Fig. 4. Calculated lattice images of V_2O_3 as a function of crystal thickness (z). (*a*) 1000 kV, $C_s = 4{\cdot}2$ mm, $\Delta f = 720$ Å, 21 reflections were recombined to form the image; (*b*) 100 kV, $C_s = 0{\cdot}7$ mm, $\Delta f = 1180$ Å, nine reflections were used; (*c*) 100 kV, the ideal phase-contrast lens was assumed, and 21 reflections were used to form the image as in (*a*); (*d*) [2$\bar{2}$01] projection of the crystal structure: open circles and small dark dots designate the columns of oxygen atoms and those of vanadium atoms respectively. The lattice spacing of {10$\bar{1}\bar{2}$} planes are shown as the scale. The projected area has the same magnification as the simulated one.

that $\sin \chi_g = -1$ for all non-zero g's and $\sin \chi_0 = 0$, that is to say, an ideal phase-contrast lens (Spence *et al.*, 1977) or the idealized propagator (Lynch, Moodie & O'Keefe, 1975) was assumed so that the smallest six spatial frequencies could be used to form the image as was the case in Fig. 4(*a*). The structure image is now obtainable but the crystal thickness is limited to about 20 Å. Therefore, firstly, the structure image obtainable at 1000 kV can be attributed to a better resolution due to the main transfer interval which is wider than at 100 kV towards the high-spatial-frequency side. Secondly, the maximum allowable thickness to obtain the structure image at 1000 kV is found at about 35 Å in the simulation Fig. 4(*a*). The ratio to the corresponding thickness in the idealized case at 100 kV (Fig. 4*c*) is ~1·7 and this is in good agreement with the value of 1·72 found for the inverse ratio ($\sigma_{100kV}/\sigma_{1000kV}$) of the interaction constant $\sigma = \pi/(\lambda E)$ (*e.g.* Cowley, 1975*a*) at the two accelerating voltages E.

3.2.2. *Phase compensation by defocus.* So far, we have assumed the Scherzer defocus or its equivalent as the defocus condition. This is not because we rely upon the weak-phase-object approximation but because these defocus conditions can be considered, being used in combination with the centred objective aperture fitted to the cut-off frequency, as a practical method of working, especially when an object of unknown structure is studied. The phase modulation due to the objective lens is, then, simple and this can help the interpretation of micrographs.

When the crystal structure is well known, defocus values more appropriate to its imaging can be deduced from the image simulation. This has already been shown by O'Keefe (1973) for large-unit-cell crystals and we can demonstrate it in the case of V_2O_3. Fig. 6 shows images calculated for different defocus values at 1000 kV under the same conditions as those in Fig. 4(*a*). Even at a crystal thickness of 60 or 80 Å a defocus value of 600 Å will give the structure image or a similar one. This will be explained as follows: the large phase shift caused by the crystal potential of those waves which form the image can be almost compensated for by decreasing the defocus value and thus the phase relation among the waves can be roughly maintained at the level of the weak-phase-object–Scherzer-defocus combination. As one can see from the simulation at $z = 80$ Å, this phase compensation is not without limit in the crystal thickness. The evolution in phase of each reflection in the dynamical scattering is more complicated than the defocus phase change, which is simply parabolic with the scattering angle, and also the evolution in amplitude with crystal thickness is, in reality, important in the image contrast.

The effect of defocus at 100 kV is shown in Fig. 7 for the crystal thickness $z = 60$ Å. Fig. 7(*a*) is calculated under the same conditions as Fig. 4(*b*), *i.e.* $C_s = 0{\cdot}7$ mm and $n = 9$. The compensation by defocus is small: $\Delta f = 1100$ Å makes $z = 60$ Å similar to $z = 50$ Å with $\Delta f = 1180$ Å. Fig. 7(*b*) shows the same calculation,

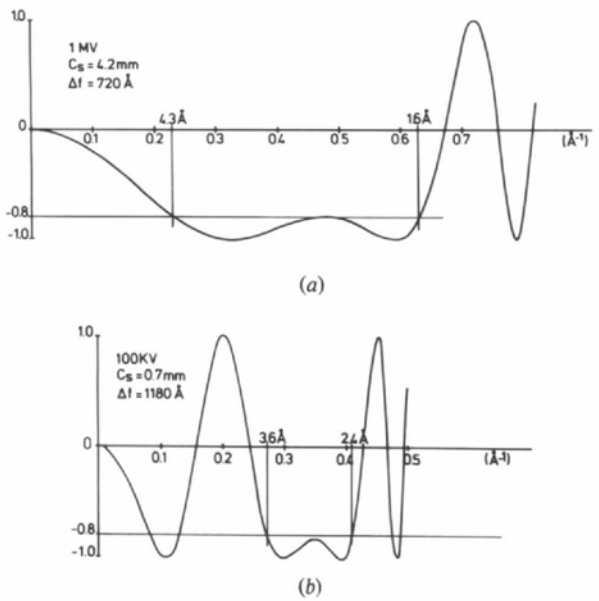

Fig. 5. Imaginary part of the transfer function, $\exp[i\chi_{g,\Delta f}]$, used in the image calculation of Fig. 4. (*a*) 1000 kV, $C_s = 4{\cdot}2$ mm, $\Delta f =$ 720 Å; (*b*) 100 kV, $C_s = 0{\cdot}7$ mm, $\Delta f = 1180$ Å.

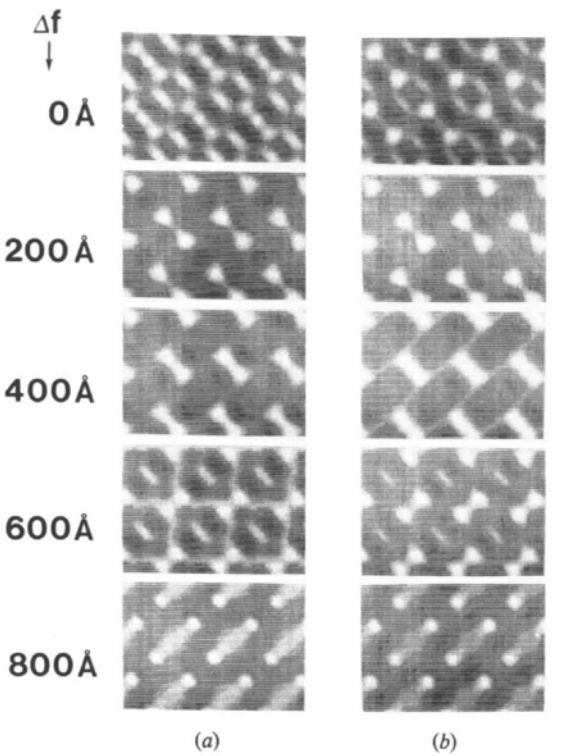

Fig. 6. Defocus series at 1000 kV with $C_s = 4{\cdot}2$ mm for crystal thickness of (*a*) 60 Å and (*b*) 80 Å. 21 reflections were recombined to form the image.

except that the objective aperture is enlarged so as to include $n = 21$ reflections instead of $n = 9$. One point must be mentioned here. At $\Delta f = 1000$ Å the columns of vanadium atoms are visible: they appear in reverse contrast as is the case for the ideal phase-contrast lens [Fig. 4(*c*), $z = 50$ Å].

3.2.3. *Incident-beam divergence and electronic instability*. These factors were not taken into consideration in the preceding calculations so that we might study purely the effect of the accelerating voltage on the lattice-image contrast.

In order to allow for the incident-beam divergence, the image intensity was calculated for nine directions, one parallel to the optic axis and eight directions on the cone of half-angle $\beta = 4 \times 10^{-4}$ rad (Krakow, 1979) to the optic axis, and then these intensities were summed up. The results are shown in Fig. 8 for $z = 60$ Å with $\Delta f = 600$ Å at 1000 kV and with $\Delta f = 1100$ Å at 100 kV and should be compared with those having the same values of defocus in Figs. 6(*a*) and 7(*a*). If the beam divergence is limited to this order, neither at 100 kV nor at 1000 kV will the lattice image be seriously disturbed.

The electronic instability can be taken into account in terms of the defocus fluctuation (Fejes, 1977). A Gaussian distribution was assumed for the fluctuations, whose standard deviation (Δ) is related to the overall electronic instability (Q) by $\Delta = C_c Q$ with the chromatic aberration constant (C_c) (Spence *et al.*, 1977). The image intensity was integrated over the distribution of defocus values thus defined. Fig. 9 shows some images calculated under the same conditions as Fig. 8 except for the beam divergence or the electronic instability. If $Q = 5 \times 10^{-6}$, the image is slightly disturbed at 100 kV and $C_c = 1$ mm (Fig. 9*c*), while the disturbance is important at 1000 kV and $C_c = 4$ mm (Fig. 9*a*). In the latter case, if $Q = 2{\cdot}5 \times 10^{-6}$ the image is not disturbed seriously (Fig. 9*b*).

3.3. *Effect of unit-cell size on the lattice-image contrast*

Lynch *et al.* (1975) have discussed on the basis of the performance of a current 100 kV high-resolution microscope the conditions permitting the intuitive interpretation of a micrograph, and have estimated that the directly interpretable resolution of about 3·5 Å is limited principally by the spherical aberration and the incident-beam divergence. Now, a 100 kV electron microscope is available with objective lenses of spherical aberration constant smaller than 1 mm. In order to evaluate the relationship between the required resolution imposed by the specimen and its maximum allowable thickness to obtain the structure image, we

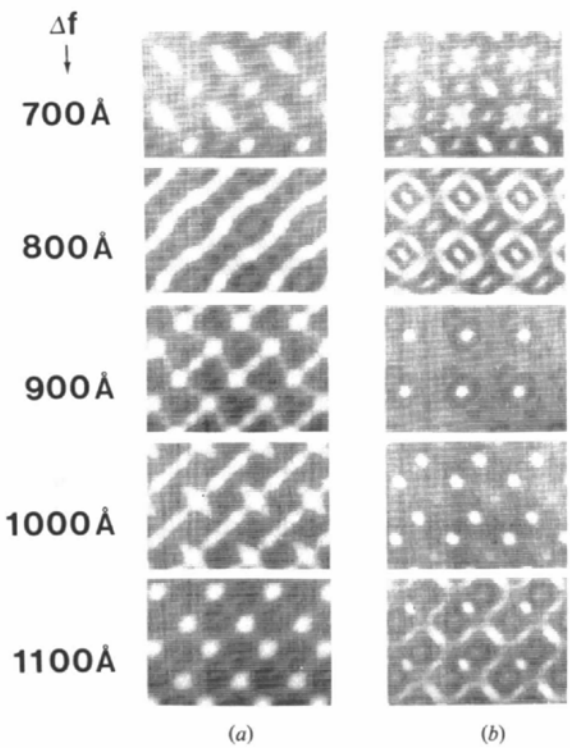

Fig. 7. Defocus series at 100 kV with $C_s = 0{\cdot}7$ mm for a 60 Å-thick crystal, with (*a*) nine reflections and (*b*) 21 reflections in the objective aperture.

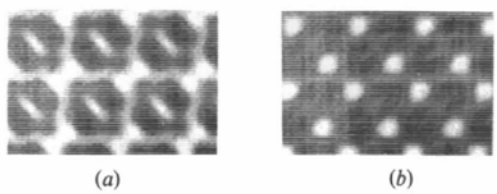

Fig. 8. Effect of the incident-beam divergence (half-angle $\beta = 4 \times 10^{-4}$ rad). Accelerating voltage, defocus value, crystal thickness and number of reflections are : (*a*) 1000 kV, $\Delta f = 600$ Å, $z = 60$ Å, $n = 21$; (*b*) 100 kV, $\Delta f = 1100$ Å, $z = 60$ Å, $n = 9$. The other conditions of image calculation are the same as those of Fig. 6 or Fig. 7.

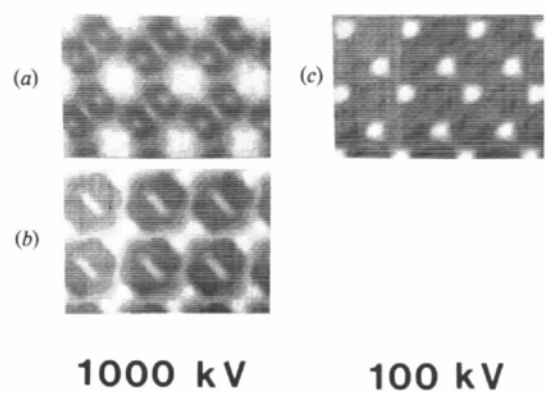

Fig. 9. Effect of the electronic instability: (*a*) $Q = 5 \times 10^{-6}$; (*b*) $Q = 2{\cdot}5 \times 10^{-6}$ at 1000 kV, $\Delta f = 600$ Å, $z = 60$ Å, $n = 21$ and $C_c = 4$ mm; and (*c*) $Q = 5 \times 10^{-6}$ at 100 kV, $\Delta f = 1100$ Å, $z = 60$ Å, $n = 9$ and $C_c = 1$ mm. The other conditions are the same as those of Fig. 6 or Fig. 7.

have, supposing a good enough resolution of the instrument, carried out lattice-image calculations at 100 kV for [2$\bar{2}$01]-oriented V_2O_3 and three model structures different from the former only in the dimensions of the unit cell. The model structures $(2/4)V_2O_3$, $(3/4)V_2O_3$ and $(5/4)V_2O_3$ have unit-cell dimensions equal to those of V_2O_3 multiplied respectively by 0·5, 0·75 and 1·25. The lattice spacing corresponding to, for example, one of the lowest reflections $10\bar{1}\bar{2}$ becomes therefore 1·828, 2·742 and 4·571 Å for these three model structures. 65 reflections were considered in the scattering matrix. The ideal phase-contrast lens (see § 3.2.1) was assumed to ensure exactly the same transfer condition of the objective lens for the four different structures. 21

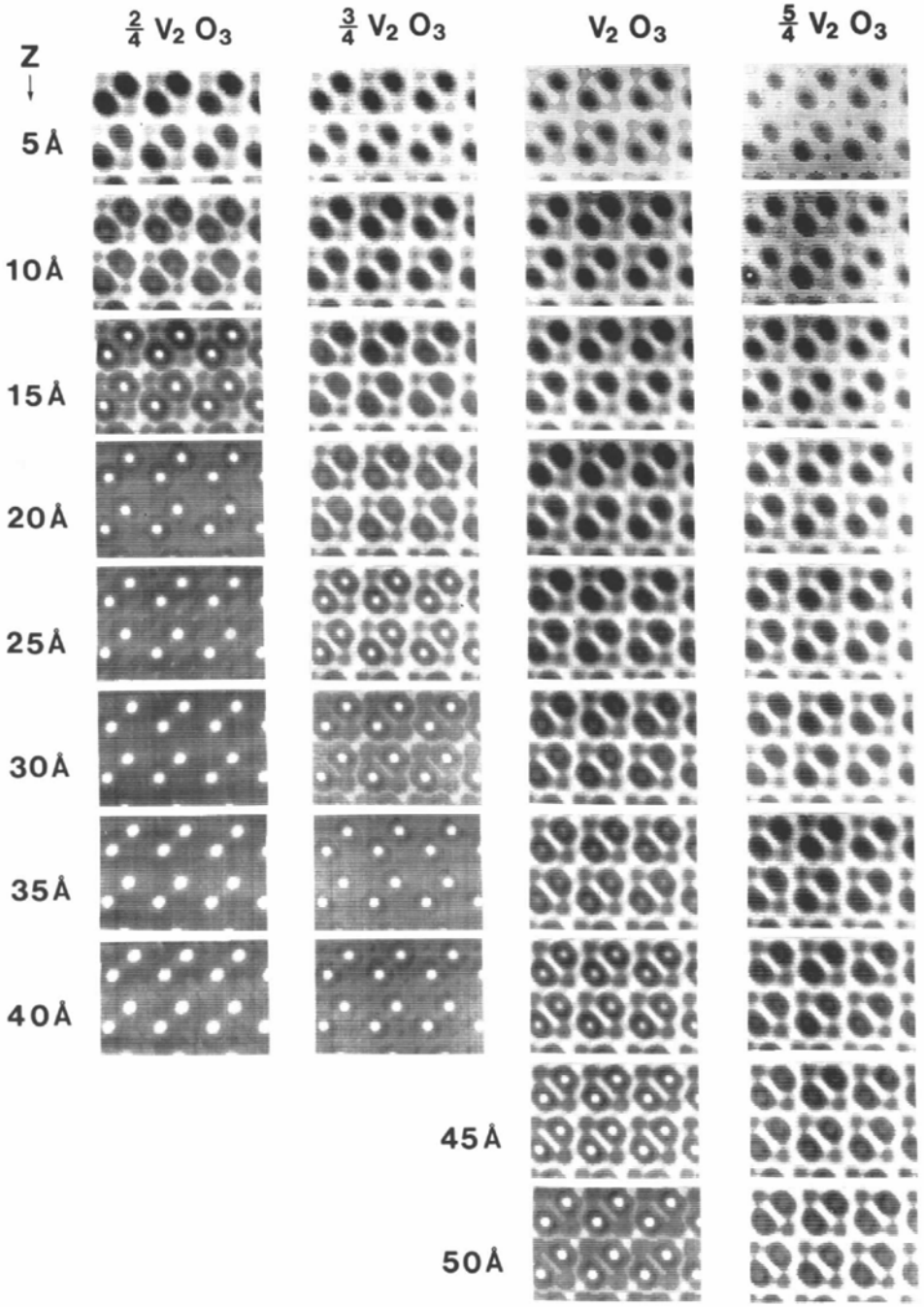

Fig. 10. Calculated lattice images of [2$\bar{2}$01]-oriented V_2O_3 crystals of different unit-cell sizes: 50% contraction (first column), 25% contraction (second column) and 25% dilatation (fourth column) from the normal unit cell (third column). 21-reflection images as a function of the crystal thickness z at 100 kV. The ideal phase-contrast lens was assumed. The magnification of each thickness series is adjusted so that images of all the four series have the same dimensions.

reflections corresponding to the lowest six spatial frequencies were used to form the images of each structure. Fig. 10 shows the four series of images calculated as a function of the crystal thickness. The magnification in the image calculation of each series is taken in such a way that the unit cell (and so the inter-column distance in the projected structure) has the same dimensions in the resulting image for the four series to facilitate comparison. For the model structure $(2/4)V_2O_3$, the image of a very thin (*i.e.* 5 Å) crystal can be referred to as the structure image, but the image of a thicker (*e.g.* 30 Å) crystal shows reverse contrast of the columns of vanadium atoms and the columns of oxygen atoms disappear, similar to the image of $\Delta f =$ 1000 Å in Fig. 7(*b*). For the other structures, the evolution of image contrast with crystal thickness is similar to that of the model structure $(2/4)V_2O_3$. However, the maximum thickness allowed to obtain the structure image increases as the unit cell becomes larger: 5–10 Å for $(2/4)V_2O_3$, 10–15 Å for $(3/4)V_2O_3$, 20–25 Å for V_2O_3 and 35–40 Å for $(5/4)V_2O_3$. Taking the mean value for each model, *i.e.* 7·5, 12·5, 22·5 and 37·5 Å, and plotting them against the unit-cell size, one can obtain Fig. 11. The thickness is normalized to that allowed by V_2O_3. The *N*-beam calculation confirms the argument from the kinematical consideration on the spread of electron beams due to Fresnel diffraction, namely it is necessary to use very thin crystals to obtain the structure image from a crystal of small unit cell. It should be noted that the maximum thickness varies more rapidly than in the linear manner represented by a straight line in the figure when the unit-cell size changes. Bourret, Desseaux & Renault (1975) have carried out image simulations at 1000 kV for (001)-oriented gold foils 50 Å thick with various deformed unit cells. Although the conditions of image formation are different from ours, mainly because of the crystal structure studied, their results are in general agreement with ours.

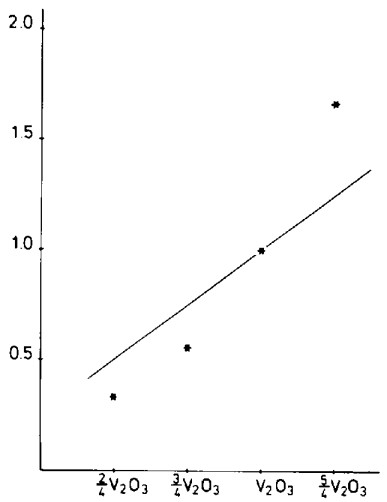

Fig. 11. Maximum allowable thickness to obtain the structure image from V_2O_3 crystals having the four different unit-cell sizes referred to in Fig. 10. The star represents the maximum crystal thickness normalized by that of the normal unit-cell crystal. The straight line indicates a linear variation with unit-cell size.

The use of the ideal phase-contrast lens – it is ideal in that the flat part of the sin χ curve is infinitely wide – enables us to study the effect of the interaction of electron beam with a crystal on the image contrast separately from the value of technical parameters such as C_s and Δf. Therefore, the essential reason for using this 'theoretical' lens is that the phase modulation due to the objective lens is exactly the same for every diffracted beam from any crystal structure, and it is secondary that $-\pi/2$ was taken as this constant value of phase shift relative to the 000 beam in order to have the normal contrast expected for a weak phase object.

4. Conclusions

In order to obtain a structure image from a small-unit-cell crystal it must be extremely thin as far as the initial structure image is concerned, which is less complicated to interpret than the structure image observed in thick regions. So the question is whether we can prepare suitable crystals. The use of high voltages will then be favourable for two reasons:

(i) The main transfer interval of the phase-contrast transfer function becomes wider toward the high-spatial-frequency side as is shown, for example, by Cowley (1975*b*). At 1000 kV the objective of $C_s = 4{\cdot}2$ mm has a transfer interval which ranges from $1/4{\cdot}3$ to $1/1{\cdot}6$ Å^{-1} and thus covers a great number of crystal structures. In other words, if the crystal is thin enough to be considered as a weak phase object, any image detail between 4·3 and 1·6 Å will be intuitively interpretable but, otherwise, as is often the case, the wide transfer interval can contribute to simplifying the image interpretation.

(ii) The interaction between the electron beam and the crystal potential is appreciably weakened, so that thicker crystals can be used in the observation. Our complete dynamical calculation shows that in the case of $[2\bar{2}01]$-oriented V_2O_3 crystal the maximum allowable thickness to obtain the structure image is relaxed from about 20 Å at 100 kV (with the ideal phase-contrast lens) to about 35 Å at 1000 kV (with $C_s = 4{\cdot}2$ mm).

It is reasonable to assume that the crystal to be treated as a weak phase object should be thinner than the maximum allowable thickness thus determined. We can also expect the structure image from a thicker crystal – which is no longer a weak phase object – provided that the structure is well known to allow the deduction of the suitable defocus value from dynamical calculations (Fig. 6).

The maximum allowable thickness increases either when the accelerating voltage increases or when the unit cell becomes larger. However, the details in the evolution of image contrast with crystal thickness are not the same for these two factors as can be seen by comparing Fig. 4(*a*) with Fig. 4(*c*). This difference is due to the dynamical interaction of Bloch waves in the crystal.

In this paper, we have discussed an accelerating voltage of 1000 kV. In fact, higher voltages such as 3000 kV can be interesting also. A recent discussion on this problem has been given by Jouffrey, Dorignac & Tanaka (1978–1979). However, as most high-voltage microscopes operate at 1000 kV, we have here chosen this voltage for our calculations.

The authors would like to express their sincere thanks to Drs A. Rocher and R. Ayroles for helpful discussions. One of us (MT) received a scholarship from the Ministry of Foreign Affairs of the French Government and this is gratefully acknowledged.

References

ANDRIANOV, G. O. & DRICHKO, I. L. (1976). *Sov. Phys. Solid State,* **18**, 803–804.

BOURRET, A., DESSEAUX, J. & RENAULT, A. (1975). *Acta Cryst.* A**31**, 746–752.

COWLEY, J. M. (1975*a*). *Diffraction Physics.* Amsterdam: North-Holland.

COWLEY, J. M. (1975*b*). *Microscopie Electronique à Haute Tension* 1975, edited by B. JOUFFREY & P. FAVARD, pp. 129–134. Paris: Société Française de Microscopie Electronique.

COWLEY, J. M. & IIJIMA, S. (1972). *Z. Naturforsch. Teil A*, **27**, 445–451.

DERNIER, P. D. (1970). *J. Phys. Chem. Solids*, **31**, 2569–2575.

DOYLE, P. A. & TURNER, P. S. (1968). *Acta Cryst.* A**24**, 390–397.

FEJES, P. L. (1977). *Acta Cryst.* A**33**, 109–113.

FEJES, P. L., IIJIMA, S. & COWLEY, J. M. (1973). *Acta Cryst.* A**29**, 710–714.

FIELDS, P. M. & COWLEY, J. M. (1978). *Acta Cryst.* A**34**, 103–112.

HALL, C. R. & HIRSCH, P. B. (1965). *Proc. R. Soc. London Ser. A*, **286**, 158–177.

HANSON, H. P., HERMAN, F., LEA, J. D. & SKILLMAN, S. (1964). *Acta Cryst.* **17**, 1040–1044.

HANSZEN, K. J. (1971). *Advances in Optical and Electron Microscopy*, edited by R. BARER & V. E. COSSLETT, pp. 1–84. London and New York: Academic Press.

HIRSCH, P. B., HOWIE, A., NICHOLSON, R. B., PASHLEY, D. W. & WHELAN, M. J. (1965). *Electron Microscopy of Thin Crystals.* London: Butterworths.

JEFFERSON, D. A., MILLWARD, G. R. & THOMAS, J. M. (1976). *Acta Cryst.* A**32**, 823–828.

JOUFFREY, B., DORIGNAC, D. & TANAKA, M. (1978–79). *Chem. Scr.* **14**, 63–73.

KRAKOW, W. (1979). *Ultramicroscopy*, **4**, 55–76.

LYNCH, D. F., MOODIE, A. F. & O'KEEFE, M. A. (1975). *Acta Cryst.* A**31**, 300–307.

O'KEEFE, M. A. (1973). *Acta Cryst.* A**29**, 389–401.

RADI, G. (1970). *Acta Cryst.* A**26**, 41–56.

REZ, P. & KRIVANEK, O. L. (1978). *Proceedings of the Ninth International Congress on Electron Microscopy, Toronto*, Vol. 1, pp. 288–289.

SCHERZER, O. (1949). *J. Appl. Phys.* **20**, 20–29.

SPENCE, J. C. H., O'KEEFE, M. A. & IIJIMA, S. (1978). *Philos. Mag.* A**38**, 463–482.

SPENCE, J. C. H., O'KEEFE, M. A. & KOLAR, H. (1977). *Optik (Stuttgart)*, **49**, 307–323.

TANAKA, M., ROCHER, A., AYROLES, R. & JOUFFREY, B. (1978). *Proceedings of the Ninth International Congress on Electron Microscopy, Toronto*, Vol. 1, pp. 286–287.

Acta Cryst. (1980). A**36**, 1041–1043

Simplified Structure Factor for MX_2-Type Compounds

BY G. K. CHADHA

Department of Physics and Astrophysics, University of Delhi, Delhi-110007, *India*

(*Received* 6 *May* 1980; *accepted* 16 *June* 1980)

Abstract

In MX_2-type structures atoms are always in a sandwich form with an M atom surrounded by two X atoms. The orientation of the M atom is always determined by the two X atoms, *e.g.* an M atom with γ orientation will always have two X atoms in A and B (or B and A) orientations around it. Therefore, by representing both X atoms by one M atom, the calculation can be reduced to one third of the original since the summation in the structure-factor calculation over all atoms will reduce to the summation over M atoms only. How this can be done is examined in the paper.

Introduction

The study of polytypism in crystals basically consists of the problem of growth mechanics and the study of

0567-7394/80/061041-03$01.00